White matter connections within the central sulcus subserving the somato-cognitive action network

Georgios P Skandalakis, Luca Viganò, Clemens Neudorfer, Marco Rossi, Luca Fornia, Gabriella Cerri, Kelsey P Kinsman, Zabiullah Bajouri, Armin D Tavakkoli, Christos Koutsarnakis, Evgenia Lani, Spyridon Komaitis, George Stranjalis, Gelareh Zadeh, Jessica Barrios-Martinez, Fang-Cheng Yeh, Demitre Serletis, Michael Kogan, Constantinos G Hadjipanayis, Jennifer Hong, Nathan Simmons, Evan M Gordon, Nico U F Dosenbach, Andreas Horn, Lorenzo Bello, Aristotelis Kalyvas, Linton T Evans

White matter connections within the central sulcus subserving the somato-cognitive action network

Georgios P. Skandalakis,[1,†] Luca Viganò,[2,†] Clemens Neudorfer,[3,4,5,†] Marco Rossi,[6] Luca Fornia,[2] Gabriella Cerri,[2] Kelsey P. Kinsman,[1] Zabiullah Bajouri,[1] Armin D. Tavakkoli,[7] Christos Koutsarnakis,[8] Evgenia Lani,[8] Spyridon Komaitis,[8] George Stranjalis,[8] Gelareh Zadeh,[9] Jessica Barrios-Martinez,[10] Fang-Cheng Yeh,[10] Demitre Serletis,[11,12,13] Michael Kogan,[14] Constantinos G. Hadjipanayis,[15] Jennifer Hong,[1] Nathan Simmons,[1] Evan M. Gordon,[16] Nico U.F. Dosenbach,[17,18,19] Andreas Horn,[3,4,5] Lorenzo Bello,[20] Aristotelis Kalyvas[8,9,‡] and Linton T. Evans[1,‡]

†,‡**These authors contributed equally to this work.**

Abstract

The somato-cognitive action network (SCAN) consists of three nodes interspersed within Penfield's motor effector regions. The configuration of the somato-cognitive action network nodes resembles the one of the 'plis de passage' of the central sulcus: small gyri bridging the precentral and postcentral gyri. Thus, we hypothesize that these may provide a structural substrate of the somato-cognitive action network.

Here, using microdissections of sixteen human hemispheres, we consistently identified a chain of three distinct plis de passage with increased underlying white matter, in locations analogous to the somato-cognitive action network nodes. We mapped localizations of plis de passage into standard stereotactic space to seed fMRI connectivity across 9,000 resting-state fMRI scans, which demonstrated the connectivity of these sites with the somato-cognitive action network. Intraoperative recordings during direct electrical central sulcus stimulation further identified inter-effector regions corresponding to plis de passage locations.

This work provides a critical step towards improved understanding of the somato-cognitive action network in both structural and functional terms. Further, our work has the potential to guide the

development of refined motor cortex stimulation techniques for treating brain disorders, and operative resective techniques for complex surgery of the motor cortex.

Author affiliations:

1 Section of Neurosurgery, Dartmouth Hitchcock Medical Center, Lebanon, NH, 03756, USA

2 MoCA Laboratory, Department of Medical Biotechnology and Translational Medicine, University of Milan, IRCCS Galeazzi Sant'Ambrogio, Milan 20157, Italy

3 Center for Brain Circuit Therapeutics Department of Neurology Brigham & Women's Hospital, Harvard Medical School, Boston MA 02115, USA

4 MGH Neurosurgery & Center for Neurotechnology and Neurorecovery (CNTR) at MGH Neurology Massachusetts General Hospital, Harvard Medical School, Boston, MA 02114, USA

5 Movement Disorder and Neuromodulation Unit, Department of Neurology, Charité – Universitätsmedizin Berlin, corporate member of Freie Universität Berlin and Humboldt-Universität zu Berlin, Department of Neurology, 10117 Berlin, Germany

6 Neurosurgical Oncology Unit, Department of Medical Biotechnology and Translational Medicine, University of Milan, IRCCS Galeazzi Sant'Ambrogio, Milan 20157, Italy

7 Geisel School of Medicine, Dartmouth College, Hanover, NH 03755, USA

8 Department of Neurosurgery, National and Kapodistrian University of Athens, School of Medicine, Athens 11527, Greece

9 Division of Neurosurgery, Department of Surgery, University of Toronto, Toronto, Ontario M5T 1P5 , Canada

10 Department of Neurological Surgery, University of Pittsburgh, Pittsburgh, PA 15213, USA

11 Cleveland Clinic Lerner College of Medicine of Case Western Reserve University, Cleveland, Ohio 44195, USA

12 Cleveland Clinic Epilepsy Center, Cleveland Clinic Foundation, Cleveland, Ohio 44195, USA

13 Department of Neurosurgery, Cleveland Clinic Foundation, Cleveland, Ohio 44195, USA

14 Department of Neurosurgery, University of New Mexico Hospital, Albuquerque, NM 87131, USA.

15 Department of Neurosurgery, University of Pittsburgh Medical Center, Pittsburgh, PA 15213, USA

16 Mallinckrodt Institute of Radiology, Washington University School of Medicine, St Louis, MO 63110, USA

17 Department of Neurology, Washington University School of Medicine, St. Louis, MO 63110, USA

18 Department of Psychological and Brain Sciences, Washington University in St. Louis, St. Louis, MO 63130, USA

19 Department of Pediatrics, Washington University School of Medicine, St. Louis, MO 63110, USA

20 Neurosurgical Oncology Unit, Department of Oncology and Haemato-Oncology, University of Milan, IRCCS Galeazzi Sant'Ambrogio, Milan 20161, Italy

Correspondence to: Aristotelis Kalyvas, MD, PhD

Division of Neurosurgery, Department of Surgery

University of Toronto

4W - 399 Bathurst Street, Toronto, ON, Canada, M5T 2S8

E-mail: aristoteliskalyvas@gmail.com

Running title: CS connections subserving the SCAN

Keywords: motor cortex; SCAN; somato-cognitive action network; Plis de Passage, white matter connectivity

Introduction

One of the fundamental tenets of structural-functional brain organization is that the primary motor cortex (M1) exhibits topographical organization arranged into somatotopic maps.[1] This conceptual framework has been widely popularized from Wilder Penfield's intraoperative direct electrical M1 stimulations which, building upon the findings by Otfrid Foerster[2] elicited isolated body-effector movements following a specific spatial pattern.[3] These findings were famously illustrated in the homunculus diagram of the motor cortex in 1948.[4] Over time, this depiction of Penfield's homunculus fostered a misapprehension that the motor cortex comprises an uninterrupted continuum of distinct motor effector-specific regions[5]—in other words, that M1 only controls the movement of certain body parts. This understanding has been instrumental and pivotal for clinicians in localizing brain lesions associated with motor deficits.[6] Nevertheless, this conventional wisdom poses challenges and has limitations, prompting further inquiry into the disruptive mechanism of action and related risks of surgical intervention in this region.[7] Stroke, a leading cause of disability, often results in motor impairments due to damage in M1 or its network connections.[6] Rehabilitation and neurostimulation techniques, such as transcranial magnetic stimulation (TMS) and transcranial direct current stimulation (tDCS), aim to enhance motor recovery by modulating M1 activity.[8,9] Additionally, M1 is crucial for surgical interventions in patients with challenging brain tumors, where advanced intraoperative mapping and meticulous planning are essential to preserve motor function, underscoring the importance of precise structural-functional knowledge of M1.[10,11] These insights also apply to the use of motor cortex stimulation therapies for neuropathic pain, epilepsy, obsessive-compulsive disorder (OCD), and other neuropsychiatric disorders, with only about half of such patients responding favorably to treatment.[7,12,13]

The primary motor cortex (M1) and the primary somatosensory cortex (S1) are crucially defined by their cytoarchitectonic features, which align with distinct anatomical landmarks such as the central sulcus. Despite some interindividual and interhemispheric variations in the superficial appearance of the central sulcus, the cytoarchitectonic boundaries that demarcate these areas show considerable consistency along the central sulcus with respect to the crests of the pre- and postcentral gyri and the fundus of the sulcus.[14] Additionally, M1 can be subdivided into '4 anterior'

(4a) and '4 posterior' (4p) subsections, based on quantitative cytoarchitecture and receptor-binding site distributions, with each subregion offering distinct functional roles.[15] This regular relationship between M1 and the gyral anatomy supports the idea that functional organization is more tightly bound to anatomical landmarks in M1 than in other cortical areas.[16]

Originally termed by Louis Pierre Gratiolet in 1854[17], plis de passage (PDP) are cortical continuations between adjacent gyri, or in other words, sulcal interruptions. Traditionally, the central sulcus PDP have been described as "connecting bridges" of cortex between the precentral (motor) and postcentral (somatosensory) gyri.[18] While Gratiolet originally described central sulcus PDP involving the motor cortex at the level of the paracentral lobule, his descriptions regarding PDP of more ventral regions of the motor cortex were vague.[17] Building on this knowledge Paul Broca subclassified PDP into 3 categories: the superior, middle, and inferior fronto-parietal PDP.[18] According to Broca, the superior and inferior PDP were more superficially situated, whereas the middle PDP ("pli de passage moyen") was located in the fundus of the central sulcus, described as transverse gyri buried within this latter structure.[18] Originally, Broca defined PDP as continua between primary motor and primary sensory cortices. More recently, other authors have termed the PDP as *continua*, with further differentiation of gyral vs. sulcal continua, the former being more superficial as visualized externally (with fused gyri as a variant), and the latter located more deeply.[19] Although the concept of PDP encompasses not only the cortical layer, but also the underlying white matter -- forming an integrated structural unit – PDP-related white matter circuits have not been thoroughly examined nor well-characterized in cadaveric or tractography studies.[20]

The 'somato-cognitive action network' (SCAN), recently described by Gordon et al. and based on precise functional MRI findings, challenged the notion of a purely motor M1 and redefined Penfield's homunculus.[21] The motor homunculus does not seem like a continuous functional gradient, but rather is interrupted by three functionally defined regions on each hemisphere, termed inter-effector regions.[21] These inter-effector regions comprise the SCAN, and are seemingly involved with movement and coordination of the entire body, distinct from the more traditional effector-specific regions that focus on isolated control of limbs, such as hands and feet, or even the mouth.[22] SCAN may constitute part of a more general action network involving integrated

body perception, pain, and action planning.[21,23] As such, SCAN sites stand in contrast to 'effector regions' dedicated to pure effector-specific motor control over specific limbs, which are structured as symmetric oval zones that, in their center, map to fingertips, toe tips, or the tip of the tongue, respectively.[21]

The SCAN operates alongside the effector-specific regions in what Gordon et al. refer to as an "integrate-isolate" pattern, where effector-specific regions isolate fine motor control (e.g., foot, hand, mouth) while the SCAN integrates broader physiological and cognitive goals.[21] The SCAN is characterized by three inter-effector regions per hemisphere, which exhibit strong functional connectivity both contra- and ipsilaterally, forming an interdigitated chain along the precentral gyrus. The pattern and location of the three inter-effector regions were consistently identified in all highly-sampled adults (Figure S1 / reprinted Figure 1 from Gordon et al 2023[21]). It was reliably replicated within individual participants across separate datasets. Additionally, this inter-effector configuration was evident in group-averaged data from large cohorts, including 4,000 participants in the UK Biobank[24]; 3,928 participants in the ABCD study[25]; 812 participants in the HCP dataset[26]; and 120 participants in the WU120 study[27] (Figure S2/ reprinted extended data Figure 1c from Gordon et 2023[21]). In contrast, the effector-specific regions demonstrate more restricted cortical connectivity to the homotopic contralateral primary motor cortex and adjacent primary sensory cortex during isolated limb movements.[21] The SCAN demonstrates strong subcortical connectivity to regions such as the centromedian nucleus of the thalamus and the cerebellum, further supporting its role in integrating motor and cognitive functions.[28,29] Moreover, the SCAN's association with internal organ control, such as connectivity to the adrenal medulla, points to its involvement in coordinating autonomic and motor responses.[29]

Both PDP and SCAN are arranged as a chain of three nodes spanning across the motor strip of the cortex. Could they have something in common? We hypothesized that PDP may provide a structural substrate of the SCAN. Here, using a comprehensive approach (Figure 1), we analyze cadaveric human hemispheres (n=16), resting-state fMRI connectomes (n ~ 9,000), and intraoperative, direct electrical stimulation recordings (n=33) to investigate and compare the structural and functional organization of the human primary motor cortex.

Materials and methods

We used a multimodal approach comprising of microdissections, fMRI, and direct electrical stimulation (Figure 1). We analyzed 16 cadaveric human hemispheres processed through the Klingler's method, using a novel sharp cortical microdissection technique to investigate the location and frequency of sulcal continua that cross the central sulcus. Given the difference in structure and similarities in distribution with the SCAN nodes, we hypothesized that these white matter connections may represent a structural substrate of the SCAN network. To that end, we manually registered locations of continua onto standard stereotactic space and used the average sites as seeds in data from three large fMRI studies — the Human Connectome Project (HCP)[26], the UK Biobank (UKB)[24], and the Adolescent Brain Cognitive Development (ABCD) Study[25] — comprising a total of approximately 9,000 subjects, to determine whether the sites of continua correspond to inter-effector regions in the SCAN network. Furthermore, we analyzed the motor output (motor evoked potentials, MEPs) recorded intraoperatively in six exceptionally rare patients who had tumors in M1/S1. During these procedures, exposure of the anterior bank of the central sulcus was required for identification and preservation of function. The analysis allowed us to reconstruct the somatotopy of the stimulated tissue, focusing on the discrimination between single-effector and multi-effector/inter-effector sites.

White matter microdissections

Sixteen normal adult cadaveric formalin-fixed hemispheres (7 right and 9 left) were prepared according to Klingler's technique, [30–32] and subsequently studied through micro-dissection of the cortex under a surgical microscope (OPMI Carl Zeiss) as previously described. Our dissection tools included various micro-dissectors, micro-forceps and micro-scissors, including arteriotomy and arachnoid 1.0/2.0 mm knives. Each dissection step in our study was conducted with approximately 1 mm thickness. Given the inherent curvature of the brain surface, dissections were performed parallel to this curvature. This method accommodates the natural anatomical contours of the brain, allowing for a more accurate morphological assessment of the structures within their native spatial relationships. In each dissection step multiple photographs were obtained from different angles using a Nikon DSLR camera with macro-lenses to adequately illustrate the

structural and topographical architecture of the PDP. In all specimens, we carried out focused cortex microdissections of the pre- and postcentral gyri. Here, we aimed to record the topography and morphology of the fronto-parietal PDP, and investigate their spatial relationships with adjacent structures of the surface anatomy including the sulci and gyri of the frontal lobe, the Sylvian fissure, and the midline (interhemispheric fissure). Left-right asymmetries were examined. We progressively dissected the cortex of the pre-and post-central gyri until the depth of the sulcus was adequately exposed. After meticulous inspection for the presence of transverse gyri, the cortex of the central sulcus was dissected until a short straight white matter connection bridging the pre- and post-central gyrus was exposed. Cortical microdissections were carried out in a stepwise manner, resembling a gradual shaving of the cortex parallel to the silhouette of the gyrus or sulcus using curved micro knives. Following exposure of the white matter connections, the surrounding cortex was dissected to illustrate the relationship between the PDP-associated white matter and the surrounding "U"-fibers. We recorded their number, topography, relationship with surface anatomy, and distance from the midline and Sylvian fissure (SF). Finally, the patterns of the PDP were reassessed, taking our results and findings into consideration.

fMRI

All PDP sites were manually registered onto the cortical surface of the template defined by the ICBM 2009b NLin Asym ('MNI') space, by identifying the corresponding site on an MNI surface atlas for each subject. Surface coordinates were averaged across cadavers to calculate a single average coordinate for each of the three PDP sites (top, middle, bottom). The mean Euclidean distance between corresponding PDP and SCAN nodes (as reported by Gordon et al.[21]) coordinates was calculated. The average surface coordinate for each of the PDP sites was used as a seed region in each of the resting-state fMRI datasets, above. Furthermore, to gain insights into the cytoarchitectonic properties underlying the identified surface coordinates, we referenced their location with the Julich-Brain Cytoarchitectonic atlas.[33]

For visualization purposes, network maps were thresholded to highlight the strongest functional connections. Due to differences in data acquisition and processing strategies employed, this

threshold varied across the datasets. Specifically, in cortex we used UKB: Z(r) > 1.0; HCP: Z(r) > 0.75; and ABCD: Z(r) > 0.1. Furthermore, because the signal-to-noise ratio of fMRI is lower in subcortical structures than in cortex, due to increased distance from the MR coil, more lenient thresholds were employed to visualize the strongest connections in subcortical structures than in the cortex. In subcortex, we used UKB: Z(r) > 0.75; HCP: Z(r) > 0.4; and ABCD: Z(r) > 0.03.

Resting-state fMRI data was averaged across participants within each of three large datasets. In brief, this approach computes pairwise correlations of activity time series between every location in the brain, thus describing the whole-brain functional connectivity pattern of every brain region. These connectivity patterns are then Fisher Z-transformed to improve normality, and averaged across participants within each dataset.

UK Biobank (UKB)

A group-averaged, weighted eigenvectors file of an initial batch of 4,100 UKB participants (ages 40-69; 53% female) -- scanned using resting-state fMRI for six minutes -- was downloaded from https://www.fmrib.ox.ac.uk/ukbiobank/. This file consisted of the top 1,200 weighted spatial eigenvectors from a group-averaged principal component analysis (PCA). Details defining data acquisition and processing pipelines are available at https://biobank.ctsu.ox.ac.uk/crystal/ukb/docs/brain_mri.pdf.[24] This eigenvectors file was mapped to the Conte69 surface template atlas[16] using the ribbon-constrained method in Connectome Workbench,[34] and eigenvector time courses of all surface vertices were cross-correlated.

Adolescent Brain Cognitive Development (ABCD) Study

Twenty minutes (4 × 5-minute runs) of resting-state fMRI data, as well as high-resolution T1- and T2-weighted images, were collected from 3,928 participants (9 to 10-years old; 51% female), who were selected as participants with at least 8 minutes of low-motion data from a larger scanning sample. Data collection was performed across 21 sites within the United States, harmonized across Siemens, Philips, and GE 3T MRI scanners. Acquisition parameters were previously described

elsewhere[25] Data processing was conducted using the ABCD-BIDS pipeline (https://github.com/DCAN-Labs/abcd-hcp-pipelines)[35]

Human Connectome Project (HCP)

A vertex-wise, group-averaged, functional connectivity matrix from the HCP 1,200 participants release was downloaded from db.humanconnectome.org. This matrix consisted of the average strength of functional connectivity across all 812 participants (ages 22-35; 410 female) who completed four 15-minute resting-state fMRI runs, and who had their raw data reconstructed using the newer "recon 2" software, with detailed acquisition and processing steps that are well-characterized in the literature.[26,34,36,37]

Intraoperative direct electrical stimulation recordings

Six patients undergoing craniotomy at the Neurosurgical Oncology Unit of Prof. Bello (IRCCS Galeazzi – Sant'Ambrogio), for resection of a cavernoma or brain tumor requiring exposure of the anterior bank of the CS, were included. Patients gave formal consent to the procedures, and the study was approved by the regional ethical committee (Lombardia 1, Italy L2093). During each procedure, the craniotomy exposed the tumor area, the central sulcus, and the adjacent pre- and postcentral gyri. During cortical motor mapping, the somatotopy of M1 on the convexity was delineated by recording motor responses to direct electrical stimulation applied to the cortical surface. The sites with the highest cortical motor threshold (cMT) (i.e. negative sites, or the ones with the lowest excitability) were used as a safe entry zone. Subcortical motor mapping guided the resection by identifying corticospinal (CST) fiber components. Motor mapping was performed, both at the cortical and subcortical level, using High-Frequency (HF) stimulation (monophasic stimulus, 500 pulse duration, ISI = 2–3 ms) delivered by a monopolar probe (straight tip, 1.5 mm diameter), combining the classical 5-shocks-mode (HF-To5) and the novel bistim-mode (HF-To2), as described in recent studies.[11,38] Upon identification of a motor response, a current-intensity curve (at 5-shocks and 2-shocks) was always performed to find threshold parameters. Tumor resection in the six selected patients required exposing a limited amount of tissue within the

anterior bank of the CS (M1), corresponding to the most caudal/posterior sector of the precentral gyrus buried within the sulcus. All surgeries were performed under general anesthesia, using propofol and remifentanil, and titrating the level of drugs to EEG and electrocorticography (ECoG) signals, to avoid any burst suppression and to maintain a continuous level of brain activity. See Supplementary Materials for details on the monitoring protocol.

MEP analysis

Raw electromyography (EMG) of contralateral and ipsilateral muscles (bilateral orbicularis oris, bilateral hemitongue, mentalis, biceps brachii, flexor carpi radialis, extensor digitorum communis, abductor digiti minimi, first dorsal interosseous, bilateral abductor pollicis brevis, quadriceps, bilateral tibialis anterior, flexor hallucis brevis) was recorded with specific software (ISIS, INOMED; sampling rate, 20 kHz; notch filter, 50 Hz). For each patient, the raw data, i.e., all the Motor Evoked Potentials (MEPs) recorded during the procedure, were extracted from the acquisition system, resampled at 4 kHz, and analyzed offline using dedicated MATLAB software. For each trial, a 100 msec window of interest from the stimulus onset was defined. The average background EMG activity and its SD (±1 SD) were then calculated from the last 25 msec of the recorded trace (i.e., from 75 to 100 msec). An MEP was considered reliable only when the EMG voltage signal exceeded the average background ±1 SD.[39] The threshold parameters and the combination of muscle responses were stored for each responsive (eloquent) site.

Reconstruction of stimulation sites

The surgical procedure was recorded through the microscope view, and MRI coordinates of all the stimulated sites were acquired by the neuronavigation system, allowing the visualization of the stimulation probe and the neuronavigation probe when applied on the effective sites, as well as the surrounding tissue and gyro-sulcal anatomy. A cortical surface extraction and surface volume registration were computed using the T1-weighted images loaded files into the neuronavigation system during surgery, using Freesurfer software.[40] Subsequently, the results were loaded onto a Brainstorm/MATLAB toolbox.[41] where the exact position of all the sites was marked as a scout

on the patient's 3D MRI. With the aid of Brainstorm, each site was co-registered to the MNI space and visualized on the 3D surface reconstruction of the anterior bank of the central sulcus (ICBM 152). The MNI coordinates of each site were used to estimate the probability of overlap with the cytoarchitectonic maps available in SPM Anatomy Toolbox.[33,42,43] The association between cytoarchitectonic maps and the type of HF-DES responses (single vs inter-effector probability values) was assessed using a Mann Whitney U-test. The region of highest probability of evoking MEPs was computed using a modified in-house version of probability kernel density estimation (PDE analysis) implemented in MATLAB.[44] Each coordinate was weighted based on the number of body-effectors involved by the stimulation, to better display the voxels associated with inter-effector responses.

Population-based High Definition Tractography

Tracts and population-based connectivity data were obtained from a population-based tractography atlas, as described by Yeh et al.[45] The atlas provided averaged trajectories for the three subdivisions of the superior longitudinal fasciculus (SLF I, II, III) across a large cohort. For brain parcellation, we employed the HCP-MMP atlas, as defined in the Glasser et al. study.[26] This parcellation scheme subdivides the cortex into 180 regions per hemisphere, enabling precise mapping of tract coverage and cortical region interactions. All visualization and data processing were conducted using DSI Studio, an open-source diffusion MRI software as previously described.[46,47] The software allowed for the integration of the tractography atlas with the HCP-MMP parcellation, enabling us to visualize and quantify the intersections between SLF subdivisions and specific cortical regions. Tract-to-region intersection probability was calculated for each hemisphere to evaluate the spatial relationships between tracts and cortical regions.

Results

White matter microdissections

A chain of three distinct, short, white matter connections (superior, middle, and inferior PDP) that interrupted the central sulcus at its depth was recorded in all studied hemispheres (Figure 1, Table S1). The PDP predominantly comprised white matter exhibiting a morphological composition, distinctly different from standard U-fibers. In contrast to the latter's delicate thinness and U shape, the white matter found within these regions exhibited a slightly deeper location, marked thickness, prominence, and a less pronounced curvature when compared to the U fibers. A satellite PDP near the inferior PDP was present in 50% of the cases. Satellite PDP adjacent to both inferior and middle PDP were present in 12.5% of the cases. A superior PDP was found at the level of the SFG in 56.25% (9/16) of the cases, at the level of the superior frontal sulcus (SFS) in 31.25% (5/16) of the cases, and at the level of the middle frontal gyrus (MFG) in 12.5% (2/16) of the cases. The average distance from the midline was 5 ± 2.6 mm. A middle PDP was found at the level of the middle frontal gyrus (MFG) in 93.75% (15/16) of the cases, and at the level of the inferior frontal sulcus (IFS) in 6.25% (1/16) of the cases. The mean distance from the midline to a middle PDP was 41 ± 15.1 mm, and from the Sylvian Fissure 37 ± 14.1 mm. An inferior PDP was found at the level of the inferior frontal gyrus (IFG) in all (16/16) of the cases. The mean distance of the inferior PDP from the Sylvian fissure was 7 ± 4.8 mm.

fMRI

Superimposing anatomically derived PDP to an MNI surface model corresponded to average coordinates of x = -58.6, y = 1.5 and z = 13.8 mm (inferior PDP); -46.1, -9.7, 46.5 mm (middle PDP); and -25.9, -22.5, 67.1 mm (superior PDP). Results are shown in Figure 2. Individual coordinates for each cadaver are reported in Supplementary Table 2 (Table S2). The mean Euclidean distance between corresponding PDP and SCAN node coordinates (as reported by Gordon et al.) was 8.89 ± 2.7 mm (mean ± SD, range: 6.2 – 11.5 mm). Seeding fMRI connectivity from these anatomically defined (PDP) average locations across three large datasets resulted in a

network pattern in every dataset (UKB: Figure 2D; HCP and ABCD: Figure S3) that precisely resembled the SCAN network, including subcortical representations, such as the centromedian nucleus of the thalamus.

To gain insights into the relationship between the anatomical location of the PDP and its underlying cytoarchitecture, we derived atlas parcellations from the Julich-Brain Cytoarchitectonic Atlas[42] and superimposed the coordinates reported by our group (Figure S4). Supplementary Table 3 (Table S3) provides an overview of the atlas allocation. Importantly, coordinates localized to border regions within primary somatosensory cortex (BA3b), primary motor cortex (BA4a), and premotor cortex (BA6), identifying the transition between areas or regions comprised of differential cell architecture.

Intraoperative direct electrical stimulation recordings

The anterior bank of the central sulcus was dissected, exposed and mapped through direct electrical stimulation in six patients (Table S4), and the MEP response of 33 eloquent sites was recorded. All stimulation sites were located on the anterior bank of the central sulcus (areas 4a and 4p). Details on stimulation parameters, effectors involved, and MEPs mean amplitude are reported in Table S5. We recorded 8 inter-effector sites within the region of the superior and middle PDP, in which direct electrical stimulation of single sites resulted in diffuse MEP responses involving muscle groups of different parts of the body. Given that these sites do not represent effector-specific regions, and to remain consistent with the current literature, we refer to them as inter-effector regions. Stimulation sites were overlapped with the 3D surface reconstruction of the anterior bank of the central sulcus/M1 at a single subject and population level (Figure 3A-G). The spatial relationship between the inter-effector sites and their probability estimation with the PDP MNI coordinates is shown in Figure 3H. Overall, we recorded 8 inter-effector sites. Three of them were recorded in patient 1. Here, direct electrical stimulation elicited reliable MEPs simultaneously in the upper limb (Extensor Digitorum Communis muscle) and the lower limb (Tibialis Anterior and Flexor Hallucis Brevis muscles) with the same threshold parameters (2 stim, 8 mA). In patient 2, HF-DES stimulation revealed an inter-effector site that, when stimulated, elicited MEPs simultaneously in the proximal upper limb (Biceps Brachi), in distal hand muscles

(Flexor Carpi Radialis, Extensor Digitorum Communis, Abductor Pollicis Brevis, First Dorsal Interosseus, Abductor Digiti Minimi) and the lower-limb district (Tibialis Anterior and Flexor Hallucis Brevis muscles). In patient 3, only single effector sites were found (upper-limb MEPs), possibly due to the limited amount of CS cortex exposed for surgical reasons, corresponding to the hand-knob sector. In patient 4, an inter-effector site was found, evoking MEPs in distal hand muscles (Flexor Carpi Radialis, Abductor Digiti Minimi) and, simultaneously, in the oro-facial district (Orbicularis Oris, Mentalis). In patient 5, inter-effector responses were recorded at three distinct sites. Here, MEPs were simultaneously evoked in distal hand muscles (Abductor Digiti Minimi, First Dorsal Interosseus) and the lower limb (Quadriceps, Tibialis Anterior). Finally, in patient 6, HF-DES of two different inter-effector sites elicited oro-facial and hand muscle MEPs (Orbicularis Oris and Abductor Digiti Minimi). We did not record any MEPs during stimulation of the inter-effector sites with current intensity below threshold parameters (i.e. the MEPs in all muscles responsive simultaneously disappeared). Finally, in an attempt to establish a more precise anatomical location of the inter- and single-effector sites within the different sub-sectors of area 4 (4a and 4p), our analysis showed no significant differences (Figure 3I).

Population-based High Definition Tractography

In this study, we utilized population-based tractography to map the trajectories and cortical coverage of the three subdivisions of the superior longitudinal fasciculus (SLF I, II, III) in relation to the precentral gyrus. We successfully reconstructed population-averaged tracts of all three subdivisions of the superior longitudinal fasciculus (SLF I, II, III) through fiber tractography and parcelated HCP-MMP cortical regions, particularly 1, 3a, 3b, and 4 (Figure S5). SLF II and III demonstrated considerable coverage over the majority of the precentral gyrus, postcentral gyrus, and portions of the central sulci, as shown in Figure S5b. Specifically, SLF I showed a more restricted intersection, primarily along the lateral portions of the precentral region. Quantitative analysis of the tract-to-region connectome (Fig. S5d) revealed high intersection probabilities for SLF II and III across the HCP-MMP regions 1, 3a, and 3b, with consistently high overlap in both the left and right hemispheres (94-100%). In contrast, SLF I exhibited minimal overlap with regions 1, 3a, and 3b, and only 6-8% overlap in the right hemisphere. In Figure (S5e), a coronal

view illustrates the distinct compartments of SLF intersection with the cortical regions. SLF II showed more medial coverage, while SLF III was predominantly lateral. This regional distinction suggests differential functional roles for SLF II and III in sensorimotor integration. Overall, these results underscore the substantial intersection of SLF II and III with precentral regions, while SLF I contributes comparatively limited (or minimal) connectivity.

Discussion

Our microdissection studies consistently revealed a chain of three distinct short white matter connections (Plis de Passage, PDP) that interrupted the depth of the central sulcus, resembling the pattern of the inter-effector regions of the somato-cognitive action network (SCAN), with a mean Euclidean distance between the SCAN nodes coordinates and the PDP coordinates of 8.89 ± 2.7 mm (mean ± SD, range: 6.2 – 11.5 mm). Seeding fMRI functional connectivity from group-averaged PDP locations in 3 large datasets (n = 9,000) functional connectomes resulted in a pattem that precisely matched the SCAN network. Central sulcus locations at which intraoperative electrical stimulation caused movement across multiple body parts (not effector specific), overlapped with the SCAN inter-effector nodes identified by functional connectivity, and the PDP identified by white matter microdissection. Our comprehensive approach utilizing microdissections, resting state MRI connectomes, and intraoperative mapping studies indicates that the PDP of the central sulcus are subserving the SCAN nodes as a structural, anatomical substrate.

Distinctive Structural Segments of the Primary Motor Cortex

Although traditional literature has focused on describing the superficial cortical folding associated with PDP,[17,18] our findings herein broaden its structural description by extending the understanding of the white matter connections within PDP architecture. This expanded view can be supported by studies that identified PDP as cortical landmarks linked with regions of increased, short-range, white matter connectivity, linking adjacent gyri; thus, PDP could be considered an integrated structural unit comprised of both gray and white matter.[20] Research has demonstrated a

concentration of short fibers in primary cortices, suggesting that PDP might represent potential key elements in the intricate network of connectivity supporting complex motor and cognitive functions.[48]

Our findings show that central sulcus PDP constitutes an interdigitated chain down the precentral gyrus, similar to the SCAN network sites described by Gordon *et al.*[21] Analogous to the newly described SCAN network loci, PDP interrupt the central sulcus, and hence M1, at specific and remarkably similar sites. We find that PDP are located within the depths of the central sulcus, reinforcing their similarity to the SCAN regions. This assertion is supported by findings of functional connectivity of the inter-effector regions into the fundus of the central sulcus.[21] The depth of the central sulcus has been implicated in proprioception,[49] a function potentially supported by the SCAN network.[21] Here, we show that PDP constitute true white matter axonal connections moving beyond traditional descriptions of unique cortical folding patterns interrupting the central sulcus. Furthermore, we highlight their role as integrated cortico-subcortical functional units. On a cytoarchitectonic level, PDP mapped to border regions within the primary somatosensory cortex (BA3b), primary motor cortex (BA4a) and premotor cortex (BA6), localizing to transition zones between cytoarchitectonic labels. This finding may indicate a possible extension of the inter-effector concept to the cytoarchitectonic level, where structure, function and cytoarchitecture could play a role in facilitating integrated body perception, action planning and execution.

Our microdissection findings demonstrate that central sulcus PDP predominantly comprise substantial volumes of white matter (Figure 1). The morphological composition of the PDP (denser, less curved, more prominent) distinctly deviates from standard U-fibers, suggesting that PDP may not connect the superficial/lateral parts of M1 and S1. PDP, as structural units, might have more extensive connectivity patterns.[48,50,51] Nevertheless, it is crucial to note that both the SCAN regions and the PDP as delineated by our dissections, do not establish connections to lateral/superficial regions of the postcentral gyrus. It is conceivable that the connection between M1 and S1 within effector-specific regions might be mediated by U-fibers, given their characteristic superficial termination patterns. Satellite connections that we often found close to the middle and inferior PDP in some of our cases, may suggest structural variations linked to case-

specific SCAN node volume differences, as reported by Gordon et al. This could indicate that in individuals with larger SCAN nodes, auxiliary PDP might be present, contributing to these subject-specific volumetric differences.

The SCAN network is characterized by its wide and extensive connectivity, mapping across various cortical regions to support complex motor and cognitive functions.[21] In contrast, PDP are more localized. Despite this apparent difference in scale, the observed similarity between the locations of PDP and SCAN nodes is compelling and suggests a potential structural basis for the SCAN's inter-effector nodes. This view is supported by research demonstrating that functional brain connectivity often reflects broader and more extensive networks than direct structural connections alone.[50,52] Studies by Honey et al. have shown that functional connectivity can emerge from indirect pathways and neural synchronization across distant brain networks, leading to broader connectivity patterns than those predicted by direct structural connections alone.[50] Similarly, Damoiseaux and Greicius emphasized that functional connectivity networks, such as those observed in resting-state fMRI, often encompass wider regions than their structural counterparts, suggesting that functional networks may be more extensive than the underlying structural connectivity.[52] Functional networks can reflect complex, dynamic interactions that extend beyond direct anatomical connections, reinforcing the idea that functional connectivity may not always align perfectly with structural connectivity.[51] Therefore, it is plausible that PDP contribute to the integrative functions of SCAN. This perspective underscores the importance of considering both cortical and white matter components when examining the structural foundations of functional networks.

Finally, in considering alternative structural networks, the presence of three inter-effector regions might superficially suggest a comparison with the three branches of the Superior Longitudinal Fasciculus (SLF). However, a more detailed anatomical analysis highlights key differences. SLF II and III are lateral to the corticospinal tract (CST), while SLF I is medial and distant from SCAN nodes as per Gordon et al.[53–55] Population-based tractography[45] further shows minimal overlap between SLF I and SCAN nodes, supporting distinct differences in their respective underlying anatomical pathways, despite some apparent superficial similarities (Figure S5).

Direct Brain Mapping: Navigating Past Challenges and Acquiring Insights

Direct electrical stimulation stands as an indispensable technique in neuroscience.[56] The conceptual framework of a motor homunculus stemmed from Penfield's intraoperative, direct electrical stimulations of the precentral gyrus.[57] However, the primary motor cortex folds within the central sulcus. It thus also occupies the anterior bank of the central sulcus which according to Penfield was not exposed during his intraoperative mapping.[58,59] Direct electrical stimulation of the anterior bank of the central sulcus requires dissection and exposure, which becomes essential when contemplating resective surgery for lesions in this region. Due to the technical complexity and inherent complication risks, lesions in this anatomical area have often been deemed inoperable. Recent advances in motor mapping strategies have challenged this view, reporting the feasibility of surgery within M1 and the corticospinal tract (CST) with a very low morbidity rate.[11,38] Our findings show that though exceptionally rare, within the context of appropriate indications and with the proper technique, the anterior bank of the CS can be exposed, and mapped through direct electrical stimulation. Moreover, our findings show that the primary motor cortex is indeed composed of effector-specific (foot, hand, mouth) motor regions and SCAN inter-effector regions important for whole-body action implementation.

The SCAN inter-effector sites were located at the transition between areas 4a and 4p, intermingled with effector-specific sites. The present data do not allow us to make conclusive remarks about a potentially different organization, in terms of somatotopy, between anterior and posterior area 4. However, our findings might suggest that the human motor system hosts a fundamental action-centered organization, or hierarchy, within its well-known effector-specific representation. This evidence is in line with both previous electrophysiological studies with direct stimulation of the human precentral gyrus convexity,[39,56] and with microstimulation (ICMS) of the non-human primate motor cortex, able to evoke ethologically relevant actions (e.g. 'bring to the mouth' movements)[28] and complex co-activation of multiple muscles, possibly supporting natural behaviors.[60] Moreover, the presence of SCAN inter-effector regions within areas 4a and 4p is consistent with recent direct mapping data obtained with intracerebral sEEG electrodes along the anterior bank of the central sulcus, which also challenge the notion of a purely body movement-

centered, human motor cortex.[22] The authors reported the existence of sites in the central sulcus, interspersed between foot-, hand-, and mouth-specific regions, that were non-specifically electrophysiologically active during movement execution with any limb; the feet, hands, and mouth. Here, we provide data confirming this newly described anatomo-functional organization by EMG recordings during direct electrical stimulation.

Expanding Beyond a Pure Motor M1 Model Reinstates Treatment Opportunities

We provide evidence on the topography, morphology and functional connectivity of the PDP of the central sulcus. Our data suggests that these connections correspond to the newly described inter-effector regions within the SCAN network. Potentially, our results add an anatomical interpretation to their functional description. The presented results further add clarity to the relationships between PDP, the SCAN network, and effector-specific motor regions in showing that PDP fall onto inter-effector regions of the SCAN network. The localization and number of PDP varies across subjects, and PDP mostly consists of white matter; thus, representing true white matter connections. This work provides a critical step towards precisely mapping the SCAN nodes through structural imaging, and could guide the development of refined motor cortex stimulation strategies and operative techniques for complex surgery of the somatomotor cortex, essential to preserve motor function.[10,11] Moreover, the SCAN was suggested to be involved in the processing of pain signals.[21] Motor cortex stimulation can treat patients with neuropathic pain, yet only 40% of patients respond to this treatment. More specific neuromodulatory targeting of the PDP might increase the therapeutic effects of M1 stimulation for the treatment of neuropathic pain, or other neuropsychiatric disorders.[7,12] Given the pivotal role of M1 in stroke rehabilitation, modulating PDP activity may also enhance motor recovery outcomes.[8,9] Furthermore, recent findings suggest that the SCAN is critically involved in the pathophysiology of Parkinson's disease and its brain stimulation treatments, making the PDP a promising candidate target for neuromodulation.[61]

Limitations and Future Directions

Despite the significant insights provided by our study, several limitations should be acknowledged. First, the sample size of cadaveric human hemispheres (n=16), while providing valuable anatomical details, may not capture the full variability present in the broader population. Second, our resting-state fMRI connectomes (n~=9,000 across three datasets) and intraoperative direct electrical stimulation recordings (n=33) provide robust functional data, yet the integration of these modalities into a cohesive model of SCAN functionality requires further validation. Third, focusing on PDP as both cortical and white matter structures is a novel perspective, but more extensive studies are necessary to fully elucidate their connectivity patterns and functional roles.

Additionally, our process of marking the PDP observed in the cadaver brains onto the template surface may have limitations. Specifically, we directly marked them on the template brain (see Figure 2, panel A). While similar processes have been used before, such as mapping histological parcellations onto the standard MNI brain[1] and lesion locations from case reports to standard MNI brain space,[5–7] it is indeed true that inter-individual variability of gyral and sulcal anatomy cannot be accounted for by this method. Our approach is more probabilistic (as described in Figure 2, Panel A), mapping average locations of the PDP (as found in cadavers) onto the average brain space (as defined by the MNI template), similar to using an average group connectome based on resting-state fMRI scans from normal brains.[12]

Regarding the imaging resolution, the fMRI scans used to create the normative functional connectome had a voxel size of between 2.0 and 2.4 mm isotropic, with no gap between slices. It is key to emphasize that the seeds were run along 812 to > 4,000 scans and the results were averaged. These datasets are widely used, and are the same group-average resting-state datasets in which SCAN was previously described by Gordon et al.[21]

Our study included motor-evoked potential (MEP) recordings following stimulations of the PDP-related sites on the central sulcus (CS). While this data is valuable, we weren't able to assess these

connections in awake patients; as such, we might have missed critical insights that could only be captured through conscious responses during specific tasks.

While our findings suggest that PDP may have implications for enhancing therapeutic outcomes in neuromodulation and surgical interventions, particularly in conditions such as neuropathic pain, Parkinson's disease and complex motor cortex-situated tumors, clinical trials and additional research are needed to confirm these potential applications. Future studies should aim to increase sample sizes, utilize longitudinal data to track changes over time, and to explore the mechanistic underpinnings of PDP involvement in broader neural networks.

Another limitation of this study is the lack of information of post-mortem times and cause of death of the donors whose hemispheres were used in the fiber microdissections. Nevertheless, when we receive cadavers in our lab, we ensure that the brains do not come from donors with neuropsychiatric disorders by excluding those with known neurological diseases or causes of death related to neurological conditions. This exclusion is based on the information provided in the official documentation we receive, which includes a log of known diseases and the cause of death as well as gross inspection of the brains. Additionally, we conduct a thorough morphological examination to confirm that there are no abnormalities or lesions indicative of gross disease or previous stroke. Cadavers that do not meet these criteria are excluded from our studies.

Data availability

fMRI data used in this study are available online (http://neuroinformatics.harvard.edu/gsp/). Patient data are available as supplementary material at Brain online. Imaging data used in this study are publicly available through the human connectome project (https://www.humanconnectome.org/) and DSI studio (https://dsi-studio.labsolver.org/). Human cadaver data are not publicly available due to conflicts with privacy reasons.

Acknowledgements

The tractographic tool used in this study is partly supported by NIH grant R01 NS120954. This work was supported by NIH grants MH096773 (NUFD), MH122066 (EMG, NUFD), MH121276 (EMG, NUFD), MH124567 (EMG, NUFD), NS129521 (EMG, NUFD), and NS088590 (NUFD); by the Intellectual and Developmental Disabilities Research Center (NUFD); by the Kiwanis Foundation (NUFD); and by the Washington University Hope Center for Neurological Disorders (EMG, NUFD). A.H. was supported by the German Research Foundation (Deutsche Forschungsgemeinschaft, 424778381 – TRR 295), Deutsches Zentrum für Luft- und Raumfahrt (DynaSti grant within the EU Joint Programme Neurodegenerative Disease Research, JPND), the National Institutes of Health (R01 13478451, 1R01NS127892-01, 2R01 MH113929 & UM1NS132358) as well as the New Venture Fund (FFOR Seed Grant). A.H. reports lecture fees for Boston Scientific and is a consultant for FxNeuromodulation and Abbott.

Funding

No funding was received towards this work.

Competing interests

N.U.F.D. has a financial interest in Turing Medical Inc. and may financially benefit if the company is successful in marketing FIRMM motion monitoring software products. E.M.G. and N.U.F.D. may receive royalty income based on FIRMM technology developed at Washington University School of Medicine and licensed to Turing Medical Inc. N.U.F.D. is a co-founder of Turing Medical Inc. These potential conflicts of interest have been reviewed and are managed by Washington University School of Medicine.

Supplementary material

Supplementary material is available at *Brain* online.

References

1. Rathelot, J.-A. & Strick, P. L. Subdivisions of primary motor cortex based on cortico-motoneuronal cells. *Proceedings of the National Academy of Sciences* **106**, 918–923 (2009).
2. Piotrowska, N. & Winkler, P. A. Otfrid Foerster, the great neurologist and neurosurgeon from Breslau (Wrocław): his influence on early neurosurgeons and legacy to present-day neurosurgery. *J Neurosurg* **107**, 451–456 (2007).
3. PENFIELD, W. & BOLDREY, E. SOMATIC MOTOR AND SENSORY REPRESENTATION IN THE CEREBRAL CORTEX OF MAN AS STUDIED BY ELECTRICAL STIMULATION1. *Brain* **60**, 389–443 (1937).
4. Gray, G. W. The Great Ravelled Knot. *Scientific American* **179**, 26–39 (1948).
5. Principles of Neural Science, Sixth Edition. https://www.mhprofessional.com/principles-of-neural-science-sixth-edition-9781259642234-usa.
6. Blumenfeld, H. *Neuroanatomy through Clinical Cases*. (Oxford University Press, Oxford, New York, 2021).
7. Hamani, C. *et al.* Motor cortex stimulation for chronic neuropathic pain: results of a double-blind randomized study. *Brain* **144**, 2994–3004 (2021).
8. Dimyan, M. A. & Cohen, L. G. Neuroplasticity in the context of motor rehabilitation after stroke. *Nat Rev Neurol* **7**, 76–85 (2011).
9. Joy, M. T. & Carmichael, S. T. Activity-dependent transcriptional programs in memory regulate motor recovery after stroke. *Commun Biol* **7**, 1–16 (2024).
10. Viganò, L. *et al.* Stimulation of frontal pathways disrupts hand muscle control during object manipulation. *Brain* **145**, 1535–1550 (2022).
11. Rossi, M. *et al.* Targeting Primary Motor Cortex (M1) Functional Components in M1 Gliomas Enhances Safe Resection and Reveals M1 Plasticity Potentials. *Cancers (Basel)* **13**, 3808 (2021).

12. Mantovani, A. *et al.* Modulation of motor cortex excitability in obsessive-compulsive disorder: An exploratory study on the relations of neurophysiology measures with clinical outcome. *Psychiatry Research* **210**, 1026–1032 (2013).

13. Hamer, H. M. *et al.* Motor cortex excitability in focal epilepsies not including the primary motor area—a TMS study. *Brain* **128**, 811–818 (2005).

14. White, L. E. *et al.* Structure of the human sensorimotor system. I: Morphology and cytoarchitecture of the central sulcus. *Cereb Cortex* **7**, 18–30 (1997).

15. Geyer, S. *et al.* Two different areas within the primary motor cortex of man. *Nature* **382**, 805–807 (1996).

16. Van Essen, D. C., Glasser, M. F., Dierker, D. L., Harwell, J. & Coalson, T. Parcellations and hemispheric asymmetries of human cerebral cortex analyzed on surface-based atlases. *Cereb Cortex* **22**, 2241–2262 (2012).

17. Gratiolet, L. P. *Mémoire sur les plis cérébraux de l'homme et des primatès: Mit einem Atlas (4 pp. XIV pl.) in fol. 33i*. (A. Bertrand, 1854).

18. Broca, P. *Mémoires d'anthropologie zoologique et biologique*. (C. Reinwald et Cie., 1877).

19. Olivier, A., Boling, W. W. & Tanriverdi, T. *Techniques in Epilepsy Surgery: The MNI Approach*. (Cambridge University Press, 2012).

20. Bodin, C. *et al.* Plis de passage in the superior temporal sulcus: Morphology and local connectivity. *Neuroimage* **225**, 117513 (2021).

21. Gordon, E. M. *et al.* A somato-cognitive action network alternates with effector regions in motor cortex. *Nature* **617**, 351–359 (2023).

22. Jensen, M. A. *et al.* A motor association area in the depths of the central sulcus. *Nat Neurosci* 1–5 (2023) doi:10.1038/s41593-023-01346-z.

23. Nico U. F. Dosenbach, Marcus E. Raichle, & Evan M. Gordon. The brain's cingulo-opercular action-mode network. Preprint at https://osf.io/preprints/psyarxiv/2vt79.

24. Miller, K. L. *et al.* Multimodal population brain imaging in the UK Biobank prospective epidemiological study. *Nat Neurosci* **19**, 1523–1536 (2016).

25. Casey, B. J. *et al.* The Adolescent Brain Cognitive Development (ABCD) study: Imaging acquisition across 21 sites. *Dev Cogn Neurosci* **32**, 43–54 (2018).

26. Glasser, M. F. *et al.* The Human Connectome Project's neuroimaging approach. *Nat Neurosci* **19**, 1175–1187 (2016).

27. Steve Petersen, Brad Schlaggar, & Jonathan Power. Washington University 120.

28. Graziano, M. S. A. Ethological Action Maps: A Paradigm Shift for the Motor Cortex. *Trends Cogn Sci* **20**, 121–132 (2016).

29. Dum, R. P., Levinthal, D. J. & Strick, P. L. Motor, cognitive, and affective areas of the cerebral cortex influence the adrenal medulla. *Proc Natl Acad Sci U S A* **113**, 9922–9927 (2016).

30. Skandalakis, G. P. *et al.* Dissecting the default mode network: direct structural evidence on the morphology and axonal connectivity of the fifth component of the cingulum bundle. *J Neurosurg* **134**, 1334–1345 (2020).

31. Skandalakis, G. P. *et al.* Establishing connectivity through microdissections of midbrain stimulation-related neural circuits. *Brain* **147**, 3083–3098 (2024).

32. Skandalakis, G. P. *et al.* Unveiling the axonal connectivity between the precuneus and temporal pole: Structural evidence from the cingulum pathways. *Hum Brain Mapp* **45**, e26771 (2024).

33. Eickhoff, S. B., Heim, S., Zilles, K. & Amunts, K. Testing anatomically specified hypotheses in functional imaging using cytoarchitectonic maps. *Neuroimage* **32**, 570–582 (2006).

34. Glasser, M. F. *et al.* The minimal preprocessing pipelines for the Human Connectome Project. *Neuroimage* **80**, 105–124 (2013).

35. Marek, S. *et al.* Reproducible brain-wide association studies require thousands of individuals. *Nature* **603**, 654–660 (2022).

36. Robinson, E. C. *et al.* MSM: a new flexible framework for Multimodal Surface Matching. *Neuroimage* **100**, 414–426 (2014).

37. Smith, S. M. *et al.* Resting-state fMRI in the Human Connectome Project. *Neuroimage* **80**, 144–168 (2013).

38. Rossi, M. *et al.* Clinical Pearls and Methods for Intraoperative Motor Mapping. *Neurosurgery* **88**, 457 (2021).

39. Fornia, L. *et al.* Functional Characterization of the Left Ventrolateral Premotor Cortex in Humans: A Direct Electrophysiological Approach. *Cereb Cortex* **28**, 167–183 (2018).

40. Fischl, B. FreeSurfer. *Neuroimage* **62**, 774–781 (2012).

41. Tadel, F., Baillet, S., Mosher, J. C., Pantazis, D. & Leahy, R. M. Brainstorm: a user-friendly application for MEG/EEG analysis. *Comput Intell Neurosci* **2011**, 879716 (2011).

42. Eickhoff, S. B. *et al.* A new SPM toolbox for combining probabilistic cytoarchitectonic maps and functional imaging data. *Neuroimage* **25**, 1325–1335 (2005).

43. Eickhoff, S. B. *et al.* Assignment of functional activations to probabilistic cytoarchitectonic areas revisited. *Neuroimage* **36**, 511–521 (2007).

44. Bellacicca, A. *et al.* Peaglet: A user-friendly probabilistic Kernel density estimation of intracranial cortical and subcortical stimulation sites. *J Neurosci Methods* **408**, 110177 (2024).

45. Yeh, F.-C. Population-based tract-to-region connectome of the human brain and its hierarchical topology. *Nat Commun* **13**, 4933 (2022).

46. Ben Shalom, D. & Skandalakis, G. P. Four Streams Within the Prefrontal Cortex: Integrating Structural and Functional Connectivity. *Neuroscientist* 10738584241245304 (2024) doi:10.1177/10738584241245304.

47. Skandalakis, G. P. *et al.* The anatomy of the four streams of the prefrontal cortex. Preliminary evidence from a population based high definition tractography study. *Front Neuroanat* **17**, 1214629 (2023).

48. Bajada, C. J., Schreiber, J. & Caspers, S. Fiber length profiling: A novel approach to structural brain organization. *Neuroimage* **186**, 164–173 (2019).

49. Krubitzer, L., Huffman, K. J., Disbrow, E. & Recanzone, G. Organization of area 3a in macaque monkeys: contributions to the cortical phenotype. *J Comp Neurol* **471**, 97–111 (2004).

50. Honey, C. J. *et al.* Predicting human resting-state functional connectivity from structural connectivity. *Proc Natl Acad Sci U S A* **106**, 2035–2040 (2009).

51. Park, H.-J. & Friston, K. Structural and functional brain networks: from connections to cognition. *Science* **342**, 1238411 (2013).

52. Damoiseaux, J. S. & Greicius, M. D. Greater than the sum of its parts: a review of studies combining structural connectivity and resting-state functional connectivity. *Brain Struct Funct* **213**, 525–533 (2009).

53. Kalyvas, A. *et al.* Mapping the human middle longitudinal fasciculus through a focused anatomo-imaging study: shifting the paradigm of its segmentation and connectivity pattern. *Brain Struct Funct* **225**, 85–119 (2020).

54. Komaitis, S. *et al.* Dorsal component of the superior longitudinal fasciculus revisited: novel insights from a focused fiber dissection study. *J Neurosurg* **132**, 1265–1278 (2019).

55. Catani, M., Jones, D. K. & ffytche, D. H. Perisylvian language networks of the human brain. *Ann Neurol* **57**, 8–16 (2005).

56. Desmurget, M., Song, Z., Mottolese, C. & Sirigu, A. Re-establishing the merits of electrical brain stimulation. *Trends in Cognitive Sciences* **17**, 442–449 (2013).

57. PENFIELD, W. THE CEREBRAL CORTEX IN MAN: I. THE CEREBRAL CORTEX AND CONSCIOUSNESS. *Archives of Neurology & Psychiatry* **40**, 417–442 (1938).

58. Penfield, W. & Welch, K. The supplementary motor area of the cerebral cortex; a clinical and experimental study. *AMA Arch Neurol Psychiatry* **66**, 289–317 (1951).

59. Penfield, W. & Welch, K. Instability of response to stimulation of the sensorimotor cortex of man. *J Physiol* **109**, 358–365, illust (1949).

60. Overduin, S. A., d'Avella, A., Carmena, J. M. & Bizzi, E. Microstimulation Activates a Handful of Muscle Synergies. *Neuron* **76**, 1071–1077 (2012).

61. Ren, J. *et al.* The somato-cognitive action network links diverse neuromodulatory targets for Parkinson's disease. 2023.12.12.571023 Preprint at https://doi.org/10.1101/2023.12.12.571023 (2023).

Figure legends

Figure 1 The plis de passage of the central sulcus. (**A**) Upper panel: Lateral view of the right hemisphere of specimen 15. The Plis de passage were superimposed on the cortex in red. The right panel highlights the intra-gyral white matter connections underlying the cortical tissue of the Plis de Passage, as revealed through the microdissection process. The inset shows an enlarged view of the middle pli de passage and a satellite middle pli de passage. Lower panel: Inferior view showing the subcentral gyrus within the sylvian fissure. A satellite inferior plis de passage was superimposed on the cortex in red. The right panel displays the white matter connection of the satellite inferior plis de passage. (**B**) Lateral view of the left hemisphere of specimen 1 showing a striking resemblance to the somato-cognitive action network (SCAN) inter-effector pattern reported by Gordon et al. in Figure 7b of their study.

Figure 2 Mapping of plis de passage sites and functional connectivity in relation to the Somato-Cognitive Action Network. (A) The plis de passage (PDP) sites of the 16 cadaver brains were mapped and manually registered onto the brain surface template (ICBM 2009b NLin Asym), by pointing to the corresponding site on an MNI surface atlas for each subject. **(B)** Coordinates were averaged across cadavers to calculate a single average coordinate for each of the three PDPs (top, middle, bottom), which were highly similar to the somato-cognitive action network (SCAN) inter-effector nodes reported by Gordon et al. [9] **(C)** Functional connectivity of each region was computed by correlating resting-state fMRI signals within these regions against the signals of

every other brain region, and then averaging these connectivity patterns across the three regions and across all subjects within UKB, HCP and ABCD datasets. **(D)** Average functional connectivity map of the three PDPs across all subjects in the UKB dataset in cortex (left) and subcortex (right). The resulting map precisely matches the SCAN described by Gordon et al.[9] See Figure S3 for a nearly identical network map in HCP, and ABCD datasets.

Figure 3 Intraoperative direct electrical stimulation sites. All stimulation sites for Patients 1-6 (A-F) are visualized on a 3D reconstruction of the anterior bank of their central sulcus and combined on the International Consortium for Brain Mapping (ICBM) 152 central sulcus template (G). Effector-specific sites are displayed in blue, while inter-effector sites (somato-cognitive action network [SCAN]) are displayed in red. (H) displays the spatial relationship between the inter-effector sites and the plis de passage (PDP) MNI coordinates as (above) and their probability density estimation (below). The three colored circles in the upper picture represent the same PDP sites from Figure 2. (I) Boxplot showing the probability of overlap between stimulation sites (inter-effector [red] vs. single-effector [blue]) for the two subsectors (anterior, posterior) of area 4. MN-U test, ns $\geqslant$ p 0.05

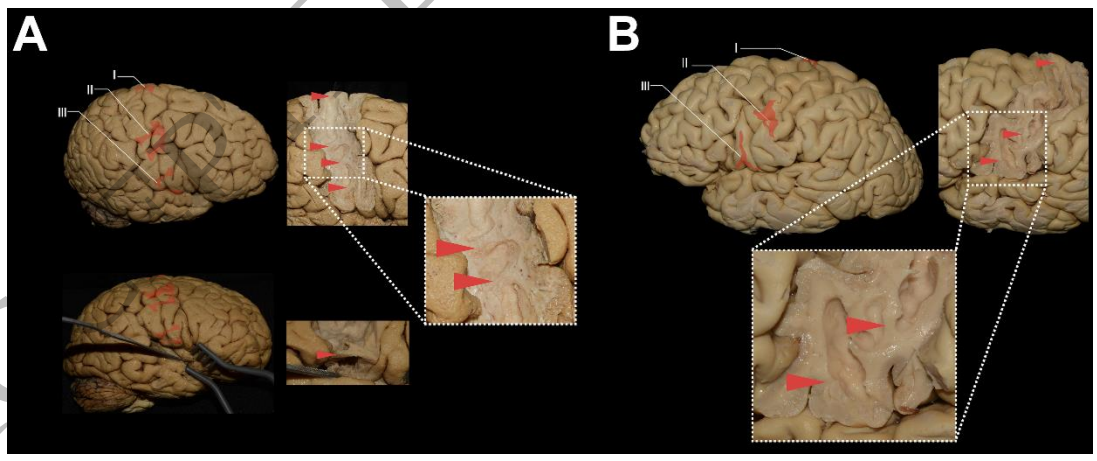

Figure 1
144x59 mm (x DPI)

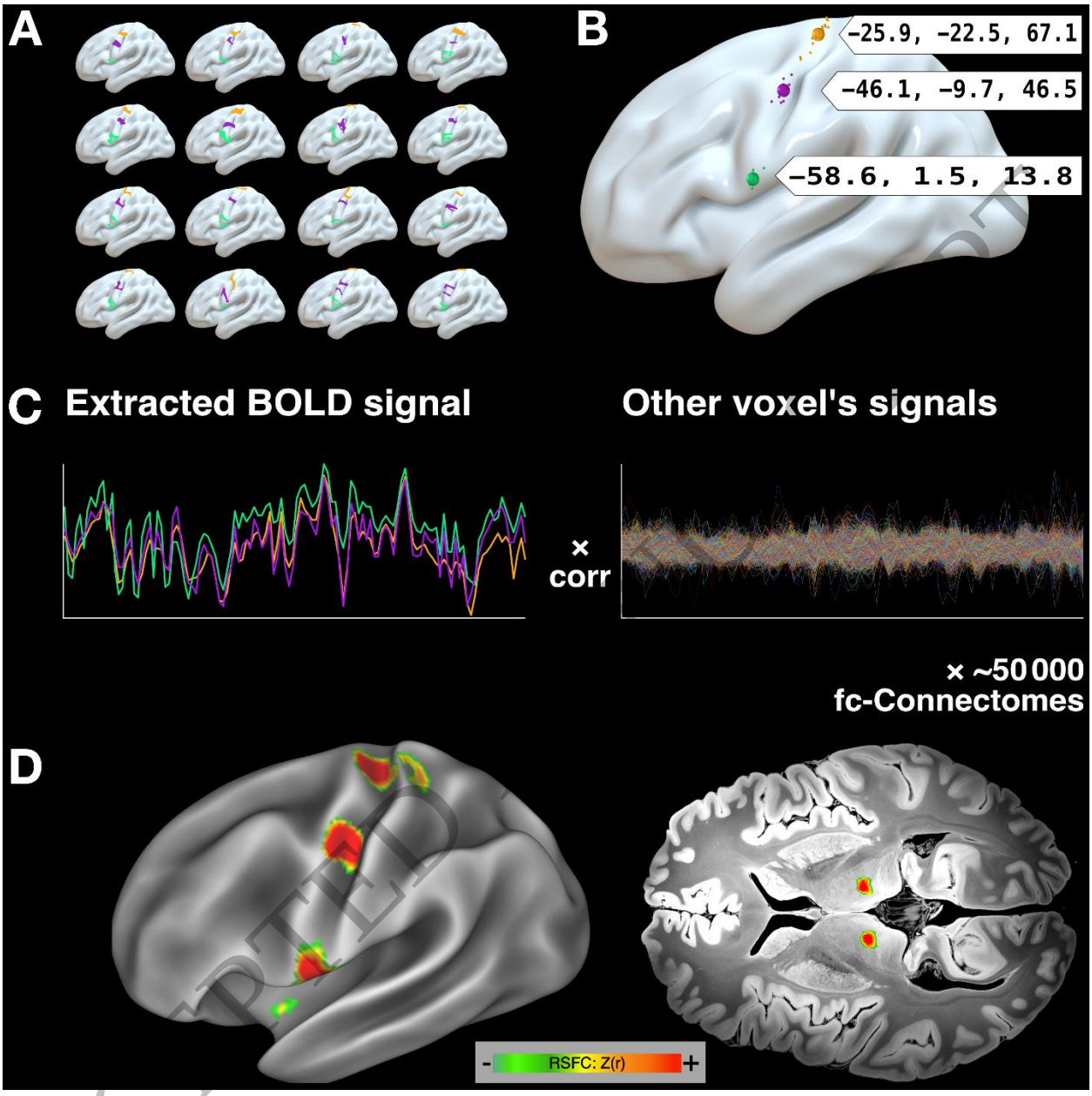

Figure 2
267x266 mm (x DPI)

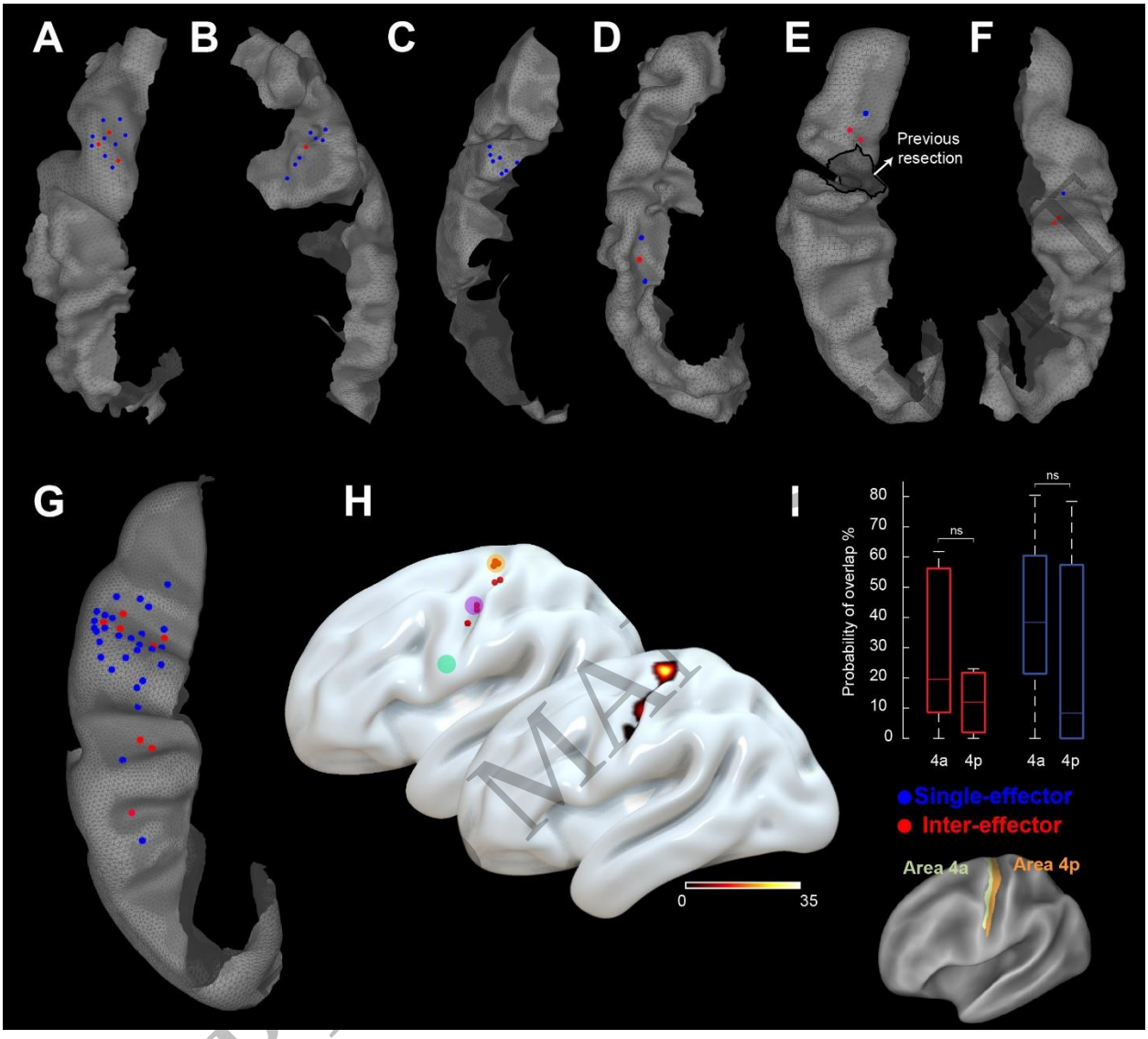

Figure 3
200x179 mm (x DPI)